






Article

# PIK3R1<sup>W624R</sup> Is an Actionable Mutation in High Grade Serous Ovarian Carcinoma

Concetta D'Ambrosio <sup>1,2,†</sup>, Jessica Erriquez <sup>1,†</sup>, Maddalena Arigoni <sup>3</sup>, Sonia Capellero <sup>1,2</sup> , Gloria Mittica <sup>1</sup>, Eleonora Ghisoni <sup>1</sup>, Fulvio Borella <sup>4</sup>, Dionyssios Katsaros <sup>4</sup>, Silvana Privitera <sup>4</sup>, Marisa Ribotta <sup>4</sup>, Elena Maldì <sup>1</sup>, Giovanna Di Nardo <sup>5</sup>, Enrico Berrino <sup>1,6</sup>, Tiziana Venesio <sup>1</sup> , Riccardo Ponzone <sup>1</sup> , Marco Vaira <sup>1</sup>, Douglas Hall <sup>7,8</sup>, Mercedes Jimenez-Linan <sup>7</sup>, Anna L. Paterson <sup>7,8</sup>, Raffaele A. Calogero <sup>3</sup> , James D. Brenton <sup>7,8</sup>, Giorgio Valabrega <sup>1,2</sup>, Maria Flavia Di Renzo <sup>1,2,\*</sup>  and Martina Olivero <sup>1,2</sup>

<sup>1</sup> Candiolo Cancer Institute, FPO-IRCCS, Candiolo, 10060 Torino, Italy; concetta.dambrosio@unito.it (C.D.); jessica.erriquez@ircc.it (J.E.); sonia.capellero@ircc.it (S.C.); mittica@aslvc.it (G.M.); eleonora.ghisoni@ircc.it (E.G.); elena.maldi@ircc.it (E.M.); enrico.berrino@ircc.it (E.B.); tiziana.venesio@ircc.it (T.V.); riccardo.ponzone@ircc.it (R.P.); marco.vaira@ircc.it (M.V.); giorgio.valabrega@ircc.it (G.V.); martina.olivero@unito.it (M.O.)

<sup>2</sup> Department of Oncology, University of Torino, Candiolo, 10060 Torino, Italy

<sup>3</sup> Department of Molecular Biotechnology and Health Sciences, University of Torino, 10126 Torino, Italy; maddalena.arigoni@unito.it (M.A.); raffaele.calogero@unito.it (R.A.C.)

<sup>4</sup> Città della Salute e della Scienza, 10126 Torino, Italy; fulvio.borella87@gmail.com (F.B.); d.katsaros@libero.it (D.K.); sprivitera@cittadellasalute.to.it (S.P.); mrribotta@cittadellasalute.to.it (M.R.)

<sup>5</sup> Department of Life Sciences and Systems Biology, University of Torino, 10125 Torino, Italy; giovanna.dinardo@unito.it

<sup>6</sup> Department of Medical Sciences, University of Torino, 10126 Torino, Italy

<sup>7</sup> University of Cambridge, Cambridge CB2 0XZ, UK; Douglas.Hall@cruk.cam.ac.uk (D.H.); mercedes.jimenez-linan@addenbrookes.nhs.uk (M.J.-L.); alp37@cam.ac.uk (A.L.P.); James.Brenton@cruk.cam.ac.uk (J.D.B.)

<sup>8</sup> Cancer Research UK Cambridge Institute, Cambridge CB2 0RE, UK

\* Correspondence: mariaflavia.direnzo@unito.it or mariaflavia.direnzo@ircc.it; Tel.: +39-011-993-3343

† These authors contributed equally to this paper.

Received: 7 November 2019; Accepted: 13 February 2020; Published: 14 February 2020



**Abstract:** Identifying cancer drivers and actionable mutations is critical for precision oncology. In epithelial ovarian cancer (EOC) the majority of mutations lack biological or clinical validation. We fully characterized 43 lines of Patient-Derived Xenografts (PDXs) and performed copy number analysis and whole exome sequencing of 12 lines derived from naïve, high grade EOCs. Pyrosequencing allowed quantifying mutations in the source tumours. Drug response was assayed on PDX Derived Tumour Cells (PDTCs) and in vivo on PDXs. We identified a *PIK3R1*<sup>W624R</sup> variant in PDXs from a high grade serous EOC. Allele frequencies of *PIK3R1*<sup>W624R</sup> in all the passaged PDXs and in samples of the source tumour suggested that it was truncal and thus possibly a driver mutation. After inconclusive results in silico analyses, PDTCs and PDXs allowed the showing actionability of *PIK3R1*<sup>W624R</sup> and addiction of *PIK3R1*<sup>W624R</sup> carrying cells to inhibitors of the PI3K/AKT/mTOR pathway. It is noteworthy that *PIK3R1* encodes the p85 $\alpha$  regulatory subunit of PI3K, that is very rarely mutated in EOC. The *PIK3R1*<sup>W624R</sup> mutation is located in the cSH2 domain of the p85 $\alpha$  that has never been involved in oncogenesis. These data show that patient-derived models are irreplaceable in their role of unveiling unpredicted driver and actionable variants in advanced ovarian cancer.

**Keywords:** ovarian cancer; PI3K; PIK3R1; Patient-Derived xenografts; PDX derived tumour cells

## 1. Introduction

Epithelial Ovarian Cancer (EOC) is a heterogeneous disease with five major histologic types [1]. The most frequent is high grade serous EOC (HGS-EOC), characterized by disruption of TP53 [2]. The majority of patients with HGS-EOC present with advanced stage disease and there has been little improvement in overall survival with standard treatment, which has not changed over the past 20 years and relies on cytoreductive surgery and platinum-based combination chemotherapy [3]. Maintenance therapy with inhibitors of the Poly (ADP-ribose) polymerase (PARP) now offers significant survival advantages for patients with BRCA1 and BRCA2 mutations [4,5], but targeted therapy for other HGS-EOC patients is much less developed compared to other solid tumours. In melanoma and non-small cell lung carcinomas, specific genetic alterations have been identified as key oncogenic drivers, i.e., as mutations able to confer a selective advantage to a cell, through either increasing its survival or proliferation and, thus, able to cause clonal expansion of the carrier cell. These findings have led to the development of therapies targeting these mutations, which has provided demonstrable clinical benefit [6]. Thus, a number of these mutations have also been defined as “actionable”, not only because their functional outcome makes carrier cells responsive to a targeted therapy, but also thanks to the availability of a specific targeted drug.

In ovarian cancer, a handful of aberrations in cancer genes have been found at high frequency, but many more cancer-related genes are found mutated at a very low frequency ( $\approx 1\%$ ) [7,8]. This so-called “long-tail” of candidate driver mutations [9] is still incompletely characterized not only in ovarian cancer but also across other human cancers [10]. Many of these mutations are not even well characterized oncogenic drivers [7,8] and evidence of the potential clinical impact is lacking.

Thus, the goal of this study is to identify driver and therapeutically actionable molecular alterations in ovarian cancer. Primarily, with this purpose in mind, we [11] and other groups [12–18] have developed platforms of Patient-Derived Xenografts (PDXs) of EOC that can recapitulate the tumour biology and clinical responses observed in donor patients. PDXs provide the most conclusive tool to validate low frequency mutations as biomarkers for targeted therapy, as evidenced by the use of colorectal cancer PDX models to predict successful clinical trials [19].

Using PDX and PDX Derived Tumour Cells (PDTC), we provide here the identification and the detailed functional and therapeutic validation of a *PIK3R1*<sup>W624R</sup> mutation found in HGS-EOC. In HGS-EOC point, mutations of genes encoding proteins of the PI3K-AKT-mTOR signalling pathway are very rare, whereas this pathway is very frequently affected by large genetic aberrations. The importance of this pathway in this and other cancer histotypes has prompted the clinical development of >40 different inhibitors [20]. However, we show here that although rare, the *PIK3R1*<sup>W624R</sup> is likely important, because it is identified as a truncal mutation in both the PDX line and source tumour. Thus, the PDX model has been instrumental in propelling the analysis, precisely because the genomic evolution of the source tumour grown in the immunodeficient animal model [21] did not counter-select this mutation. Moreover, we show here that the PDX model has been invaluable for functional validation, as it allowed overcoming questionable assays in test tubes or in unrelated cell types.

## 2. Materials and Methods

### 2.1. Cell Lines

The OVCAR-8 (NCI-DTP Cat# OVCAR-8) were obtained from the NCI-DCTD repository. The A2780 (NCI-DTP Cat# A2780) ovarian carcinoma cells lines and the LNCaP prostate carcinoma cell line (CLS Cat# 300265/p761\_LNCaP) were purchased from American Type Culture Collection (ATCC). Cell cultures were maintained following the protocols suggested by the providers.

### 2.2. Patient-Derived Xenograft (PDX) Platform

Between 2012 and 2016, a collection of 167 separate clinical samples of epithelial ovarian cancers was undertaken, with the understanding and written consent of each subject before they participated in

the study, and according to the PROFILING Protocol, and it also conformed to the standards set by the Declaration of Helsinki, and was approved by the Regione Piemonte Ethical Committee (approval number 5141 on 9/3/2011), and then by the IRCCS Ethical Committee (approval number 192/2016 on 19/7/2016).

Samples have been implanted intra-peritoneum and subcutaneously in the right flank of severely immunocompromised NOD/Shi-scid/IL-2R  $\gamma$ null mice and subsequently propagated subcutaneously, based on our and other authors' data showing that the continued development of the PDX model subcutis was suitable [11,12]. Sample quality was assessed by the pathologists. A total of 65 PDX lines successfully grew (thus with an approximate take of 40%) and were propagated for at least three passages. Table S1 shows the full characterization of tumours and a quality assurance of 43/65 PDX lines, carried out in accordance with Meehan et al. [22] within the first three passages of PDX lines, which resulted in loss of human stroma. For treatment, animals were randomized using the Laboratory Assistant Suite [23]. Animal treatment was initiated when mean xenograft volume was approximately 100 mm<sup>3</sup>. Buparlisib diluted in N-Methyl-2-pyrrolidone and PEG 10/90 *v/v* was administered by oral gavage every day 5 days/week for 3 weeks. Buparlisib was administered at the dose of 20 mg/kg, that was reported to be effective in diverse PDX models [24]. Treatment with buparlisib at doses >30 mg/kg resulted in mouse toxicity. Control animals were treated with vehicle alone. All animal procedures were approved by the local Ethical Commission and by the Italian Ministry of Health in accordance with EU Directive 2010/63/EU for animal experiments; a first authorization was obtained on 12/7/2012 and, following subsequent regulations, approved again on 14/01/2016 (no. 16/2016-PR) and extended for two additional years on 17/9/2018. All animal procedures comply with the "3R" principles. Additional methodological details of animal experimentation are reported in Supplementary Methods Part 1. The completed ARRIVE guideline checklist for reporting experiments using live animals is attached as Supplementary Methods Part 2.

### 2.3. TMAs and IHC

Tissue Microarray (TMA) preparations and staining were carried out as described by Sapino et al. [25] TMA slides for the characterization of the PDX lines were stained with the Ventana automated immunostainer (BenchMark AutoStainer, Ventana Medical Systems, Tucson, AZ, USA) using the following antibodies by Ventana Medical Systems: anti-WT1 Cat# 760-4397, anti-p53 Cat# 790-2912, anti-EPCAM Cat# 760-4383, anti-Cytokeratin 7 Cat# 790-4462 and anti-CD20 Cat# 760-2531, the latter to rule out the growth of lymphoma, which occurred in 10–20% of cases, as also reported by others [26]. Immunohistochemical detection of S6 and P-S6 in TMA slides of PDXs was carried out using rabbit monoclonal antibodies (Cell Signalling Technology; Denver, MA, USA) Cat# 2217 and Cat# 4858, respectively, and anti-rabbit Ig (K4003) and EnVision system purchased from Dako (Agilent, Santa Clara, CA, USA). The immunohistochemical detection of Ki67 and P-S6 in sections of PDXs was carried out using mouse monoclonal (Dako clone MIB-1) and rabbit monoclonal antibodies (Cell Signalling Technology Cat# 4858) respectively, anti-mouse or anti-rabbit Ig (K4001 and K4003, respectively) and EnVision system purchased from Dako (Agilent, Santa Clara, CA, USA). Quantification of P-S6 and Ki67 positive cells was carried out using the Colour Deconvolution plug-in in ImageJ in 20–30 and 10–15 separated fields, respectively, of each PDX.

### 2.4. PDX Derived Tumour Cell (PDTC) Preparation

PDX samples have been chopped and digested with a Human Tumour Dissociation Kit (Miltenyi Biotec, Bergisch Gladbach, Germany) according to the manufacturer protocol. Human cells were isolated using a Mouse Cell Depletion Kit (Miltenyi Biotec). Cells were plated, and after 24–48 h treated with a drug in 96-multiwell plates.

### 2.5. Viability and Cytotoxicity Assays

A CellTiter-Glo<sup>®</sup> assay was used to evaluate the viability of PDTCs and cell lines after 72 h treatment with drugs, according to the manufacturer's protocol (Promega, Madison, WI, USA). Drugs were purchased

from Selleck Chemicals (Houston, TX, USA). GR values have been calculated for each concentration as reported in Hafner et al. [27] and plotted using a GraphPad Prism version 7.02 (San Diego, CA, USA).

A cytotoxicity assay was carried out as follows. Seventy-two hours after treatment, cells in 96-well plates were fixed with 2% paraformaldehyde in PBS for 40 min, washed twice in PBS and stained with 10% crystal violet in 20% methanol for 40 min. Plates were washed extensively and lysed in 10% acetic acid. The absorbance was measured at 595 nm using a microplate reader (BioTek Synergy HTX, Winooski, VT, USA).

### 2.6. Western Blot Analysis

PDTCs were treated for 24 h with the indicated drug or the vehicle 24 h after plating. From PDTCs and PDX samples, proteins were extracted in ice cold elution buffer (TrisHCl pH 7.4, containing EDTA, 1% Triton X-100, 10% glycerol and protease and phosphatase inhibitors). Proteins of snap frozen PDXs have been extracted as above after GentleMacs (Miltenyi Biotec) digestion. Western blot (WB) analysis was carried using the following antibodies: rabbit polyclonal anti-AKT (Cell Signalling Technology Cat# 9272), rabbit monoclonal Phospho(Ser473)-AKT (Cell Signaling Technology Cat# 4060) and polyclonal goat anti-vinculin (N-19) (Santa Cruz Biotechnology Cat# sc-7649). Labelled secondary antibodies have been revealed with ECL (Thermo Fisher Scientific, Waltham, MA, USA) using the ChemiDoc Touch Imaging System (BioRad, Hercules, CA, USA).

### 2.7. Crystal Structure Analysis

The position of W624 residue in the structure of human p85 $\alpha$  encoded by *PIK3R1* was predicted through sequence alignments and structure superimposition. Sequence alignments and domain assignment were performed using PSI-Blast (NCBI BLAST), whereas structure superimposition was performed using UCSF Chimera.

### 2.8. WES and CNA Analysis

Exome library preparation was performed using the Nextera Rapid Capture Enrichment kit from Illumina. Genomic DNAs were quantified using the Qubit system (Invitrogen, Carlsbad, CA, USA) and 50 ng were used as input material for library preparation. Pools of 12-plex libraries (500 ng each library) were hybridized with capture probes (coding exomes oligos) twice: a first hybridization step for 2 h and a second for 18 h. After elution and clean up, enriched DNA libraries were amplified with 10-cycle PCR. The products were purified, loaded on a bioanalyser using DNA 1000 chip for quality control and quantified with Qubit. Samples were sequenced using the NextSeq 500 platform (Illumina, San Diego, CA, USA) as paired 150 bp reads, using the NextSeq 500/550 High Output Kit v2, loading 1.4 pM DNA and obtaining as cluster density an average of 200 K/mm<sup>2</sup> clusters. Microarray HumanCytoSNP for CNA analysis was performed by Genomix4life S.R.L. (Baronissi, Salerno, Italy), using 200 ng of each DNA hybridized for 18 h at 48 °C on HumanCytoSNP-12 v2.1 BeadChip, according to the manufacturer's instructions, and analysed with an Illumina iSCAN. WES and SNP data analyses were performed using the pipeline shown in Figure S1, using each patient's germline DNA as reference. The data generated or analysed during this study are included in this article, or if absent, are available from the corresponding author upon reasonable request.

### 2.9. Pyrosequencing Analysis

The presence and allele frequency of *TP53* and *PIK3R1* mutations in source tumours of any PDX line were assessed using pyrosequencing (QIAGEN, Hilden, Germany). Briefly, sample DNAs were amplified, and the PCR products were subjected to the 'sequence by synthesis' pyrosequencing method following the manufacturer's instructions, using the primers and conditions reported in Table S5. Results were analysed with the PSQ24 software for allelic quantification.

### 3. Results

#### 3.1. Mutational Burden of PDX Lines from HGS-EOCs

Forty-three PDX lines derived from epithelial ovarian carcinomas were fully characterized according to the minimal information standard for reporting PDX data [22], including clinical and pathological attributes of the patient's tumour, the processes of implantation and passaging in the host mouse strain, and quality assurance by means of genotypic and phenotypic characterization. The information is reported in Table S1. Briefly, we compared the histology of each PDX to that of the source tumour and classified histotype using immunohistochemistry (IHC) with CK7, EPCAM, WT1 and p53 antibodies, which confirmed the diagnosis of high grade serous histology in 25/43 lines. Figure 1 shows the histology and IHC staining of TMAs of representative PDX lines and the corresponding source tumours. Targeted NGS of *TP53* showed that all the PDXs from HGS-EOC harboured *TP53* mutations (Table S1). *TP53* aberrations were protein truncating or missense mutations previously shown to be pathogenic according to the IARC *TP53* Database (<http://p53.iarc.fr/>). The detailed list of aberrations is reported in Table S1. Samples with missense mutations in *TP53* had evidence of nuclear p53 stabilization as indicated by high protein expression in tumours and xenografts (Table S1). The PDX line with null splice site mutation did not express p53 protein. The targeted NGS of *BRCA1/2* showed mutations of these genes classified as likely pathogenic according to the BRCA Mutation Database (<http://arup.utah.edu/database/BRCA>) in 19% of the above PDX lines, i.e., close to the expected frequency. The likely impactful aberrations and the variants of unknown significance detected in the 43 PDX lines are listed in Table S1.

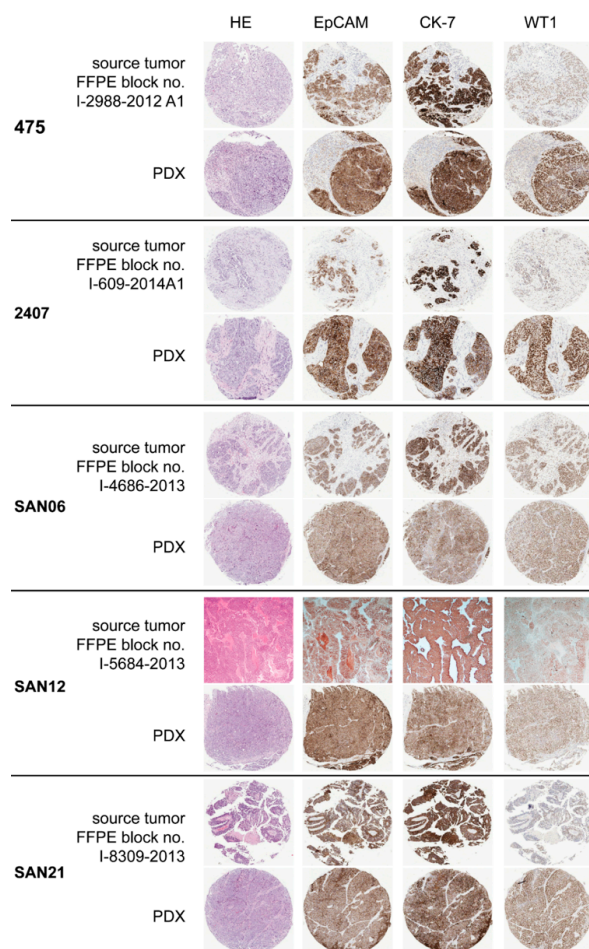


**Figure 1.** Histological characterization of PDX lines. Representative images of TMAs of PDX lines compared to sections of the corresponding source tumours. Numbers on the left are those of PDX lines as catalogued by the PROFILING approved protocol, while the numbers of the used FFPE block of samples of source tumours are shown on the top left of each panel. The complete characterization of these and the other thirty-eight PDX lines is reported in Table S1.

We then further studied 12 PDX lines propagated from treatment naïve HGS-EOCs, listed in Table S2, that also reports clinical information.

In the 12 PDX lines, using Whole Exome Sequencing (WES), we detected a total of 2743 single nucleotide variants (SNVs) in 2314 genes. The majority (79%) of mutated genes in our analysis have been reported as mutated in the TCGA analysis of 523 HGS-EOC [8]. Most (438/487) of the mutated genes not listed in the TCGA analyses of HGS-EOC have been found mutated in other cancer histotypes, according to the Pan-Cancer Atlas.

*TP53* was the only gene mutated in all 12 PDX lines, and the only gene found mutated across more than one PDX line (Table S1), with an allele frequency of approximately = 1, in line with occurrence of LOH. As expected, in the studied 12 PDX lines, WES detected the same *TP53* mutations identified with targeted NGS.

### 3.2. Somatic *PIK3R1*<sup>W624R</sup> Mutation in HGS-EOC

To identify possible driver and actionable genetic aberrations in the 12 above-mentioned PDX lines, we considered SNVs and copy number alterations (CNAs) affecting cancer-related genes reported in COSMIC (CGCv84) [28].

CNAs detected in cancer genes corresponded to those reported in TCGA for HGS-EOC (Table S3A). Among genes reported in TCGA as amplified in more than 10% of cases [29], in our small series (Table S3B) we found the expected frequency of increased copy number of *CCNE1* and *PIK3CA*. LOH of the *TP53* gene in each of the PDX lines was confirmed (compare the data of Tables S1 and S2).

The list of cancer genes harbouring SNVs in the 12 PDX lines is shown in Figure 2 and Table S4.

It came out that, in 3/12 PDX lines, WES did not detect mutations in known cancer genes other than *TP53*. A number of SNVs in cancer genes were identified as Single Nucleotide Polymorphisms (SNPs). All the variants are listed in Table S4. Only some of the somatic mutations in the remaining 9 PDX lines were predicted to be damaging and/or deleterious based on the bioinformatics tools used for analysis (Figure 2, SIFT, PROVEAN and FATHMM [30]). Possible actionability (Figure 2) was evaluated using the Drug Gene interaction database (DGidb) [31].

In the PDX line #475, we found a point mutation of the *PIK3R1* gene that results in the W624R residue substitution in the encoded protein. This was detected with an allele frequency approximately = 1.0, which suggested that this was a loss of function mutation followed by LOH, in accordance with *PIK3R1* classification as a tumour suppressor gene. As explained above, based on the bioinformatic tools (see Figure 2), this mutation was predicted to be deleterious and damaging and possibly actionable. *PIK3R1* encodes the p85 $\alpha$  regulatory subunit of the p110 $\alpha$  catalytic subunit of the Phosphatidylinositol-3 Kinase (PI3K). Some of the already known mutations of the p85 $\alpha$  subunit affect the intracellular signalling of the PI3K pathway, leading to PI3K activation, via distinct molecular mechanisms [32]. Activation of the PI3K pathway in this PDX line #475 was shown by the immunohistochemical detection of the phosphorylation of the S6 protein, that is a proxy of AKT activation (Figure S2). In other PDX lines, without mutations of genes involved in the PI3K/AKT/mTOR pathway, the P-S6 protein is not comparably increased (Figure S2).

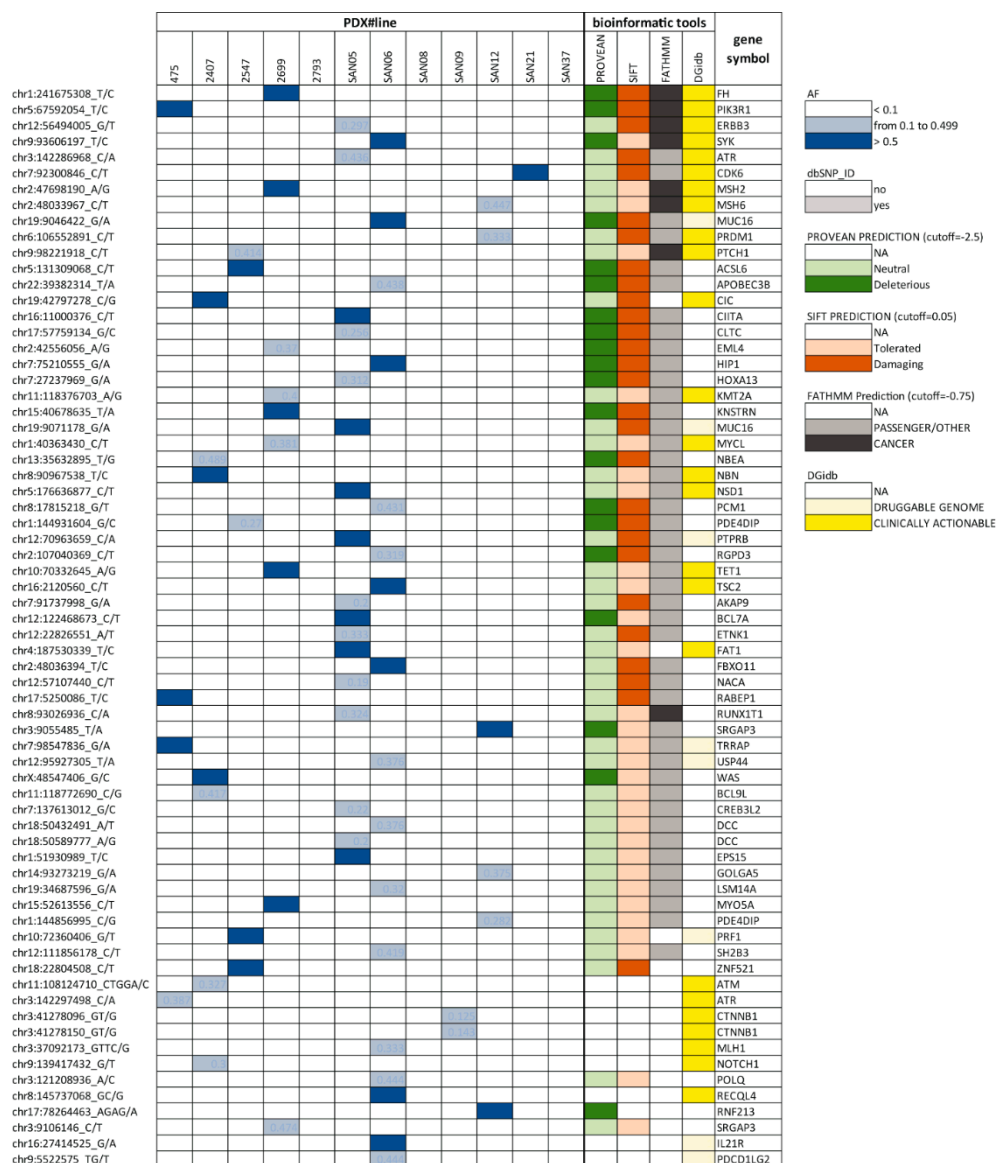


**Figure 2.** Single Nucleotide Variants (SNVs) in cancer genes found in PDX lines derived from naïve HGS-EOC. Variants with an allele frequency (AF)  $\geq 0.1$  are listed. Only SNVs not classified as SNPs based on the SNP database are shown in this Figure 2. All the variants, including those classified as SNPs, are reported in the related Table S4. Legend to boxes is shown on the right.

*PIK3R1*<sup>W624R</sup> was detected in all the parallel and sequential passages of the PDX line #475 and in each passage with an allele frequency approximately = 1.0. In these passages also, the same *TP53* mutation was found with an allele frequency approximately = 1.0, in line with *TP53* mutation being a truncal mutation, as previously shown (see e.g., ref. [33]). Thus, data suggested that the *PIK3R1*<sup>W624R</sup> might also be a truncal mutation in PDXs. Most other mutations were also consistently detected in all passages of this PDX line, whereas only a few were limited to a subset of passages. The list of public, shared and private mutations found in passages is shown in Figure 3A. The consistency of public SNVs in parallel and sequential passages demonstrated the genetic stability upon passages of the PDXs carrying the *PIK3R1*<sup>W624R</sup> mutation.

The *PIK3R1*<sup>W624R</sup> PDX line was propagated from a biopsy sample taken at laparoscopy from a patient with a stage IIIc HGS-EOC. This PDX line responded as well as the patient to platinum-based chemotherapy. Indeed, the patient received neo-adjuvant platinum-based chemotherapy followed by surgery. Regrettably, the patient relapsed after six months and received a second platinum-based

line that came out to be limitedly effective. At post-chemotherapy surgery, another sample was propagated as the PDX line, which no longer responded to carboplatin. In this paired PDX line the *PIK3R1*<sup>W624R</sup> mutation was also found with an AF approximately = 1. More importantly, we found the same *PIK3R1*<sup>W624R</sup> mutation in specimens of the source tumour. Pyrosequencing of two distinct FFPE samples of the source tumour showed that in each FFPE sample the percentage of the *PIK3R1*<sup>W624R</sup> sequence was the same as that of the *TP53* allele found mutated in the PDX line (panels B–E of Figure 3). The percentage of the mutated *TP53* allele was considered a reliable proxy of the percentage of tumour cells in the source tumour specimens.

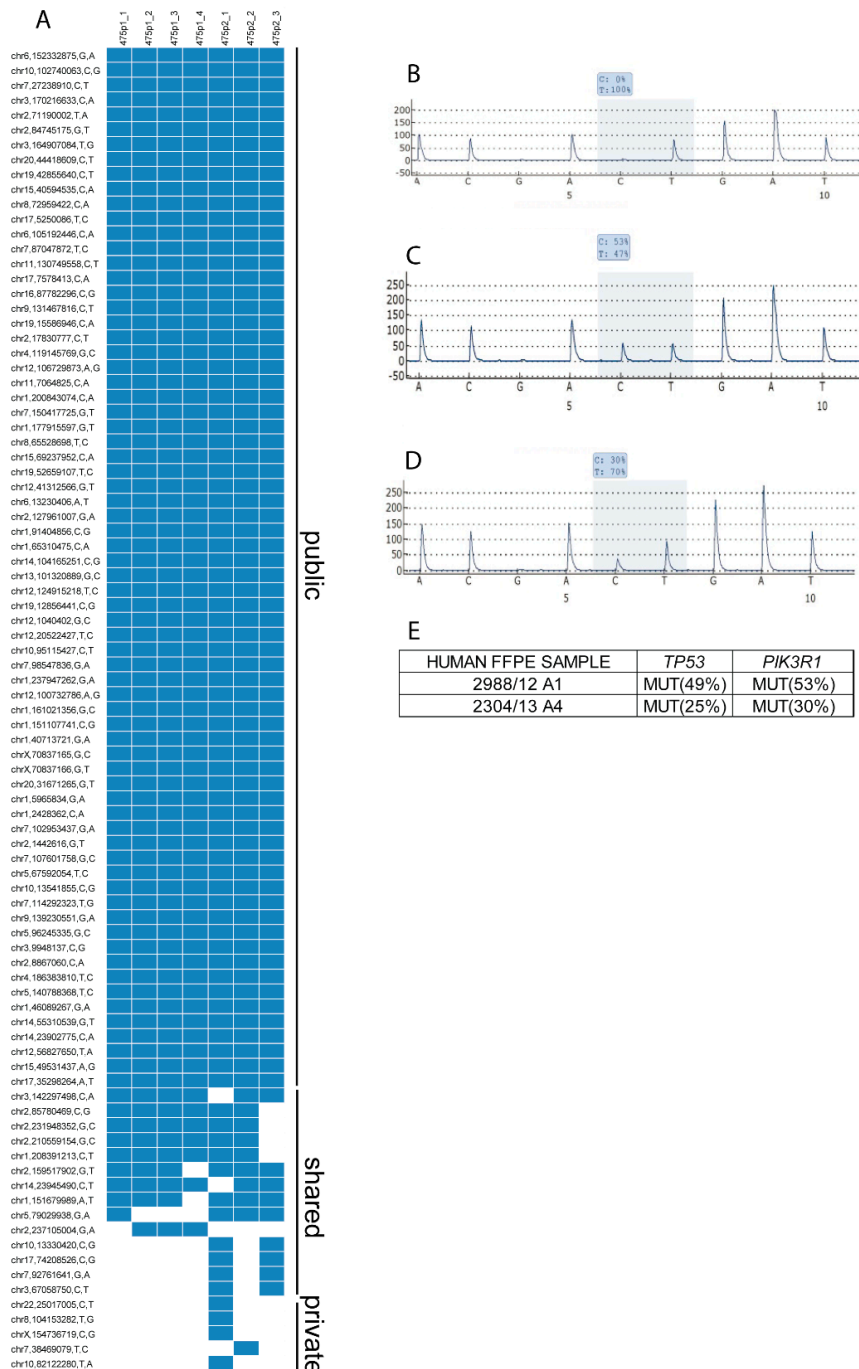


**Figure 3.** Identification of the *PIK3R1*<sup>W624R</sup> mutation as truncal mutation in parallel and serial passages of the PDX line #475 and in the corresponding source tumour. (A) The W624R mutation in *PIK3R1* is



one of several public mutations found in seven parallel and serial passages of the PDX line#475. (B–E) Pyrosequencing analysis confirmed the presence of the *TP53* and the *PIK3R1* mutations found in the #475 PDX line in two FFPE samples from distinct blocks of the source tumour. The *TP53* and the *PIK3R1* mutated sequences showed the same allele frequency (AF) in each sample. The AF of the PDX line-specific *TP53* mutation was considered as a proxy of the percentage of tumour cells in the human tumour samples. (B) Sequence of *PIK3R1* in Control Reference Genome; (C) percentage of *PIK3R1*<sup>W624R</sup> in FFPE sample A1 from the paraffin block 2998 of the source tumour; (D) percentage of *PIK3R1*<sup>W624R</sup> in FFPE sample A4 from the paraffin block 2304 of the source tumour; (E) percentage of mutated sequences of *TP53* and *PIK3R1* in the two above FFPE samples.

### 3.3. Ex Vivo and In Vivo Assays of *PIK3R1*<sup>W624R</sup> Actionability

As mentioned above, to estimate the therapeutic implications of any given mutation, we first used the Drug Gene interaction database (DGidb) [31] that suggested the actionability of *PIK3R1*<sup>W624R</sup>. Another resource, the DEPO database (Database of Evidence for Precision Oncology, <http://depo-dinglab.ddns.net/>), that focuses on specific mutations for therapeutic projections, was not useful because it does not report hotspot regions of the *PIK3R1* gene. However, we focused further attention on this mutation because of the potential actionability of a member of the PI3K-AKT-mTOR pathway.

Hypothesis on the functional role of any given mutation can also be formulated based on crystal structures of the molecules and complex of interest. Thus, we investigated the possible role of the W624R mutation in the interaction between the p85 isoforms and p110 isoforms of PI3K (Figure 4).

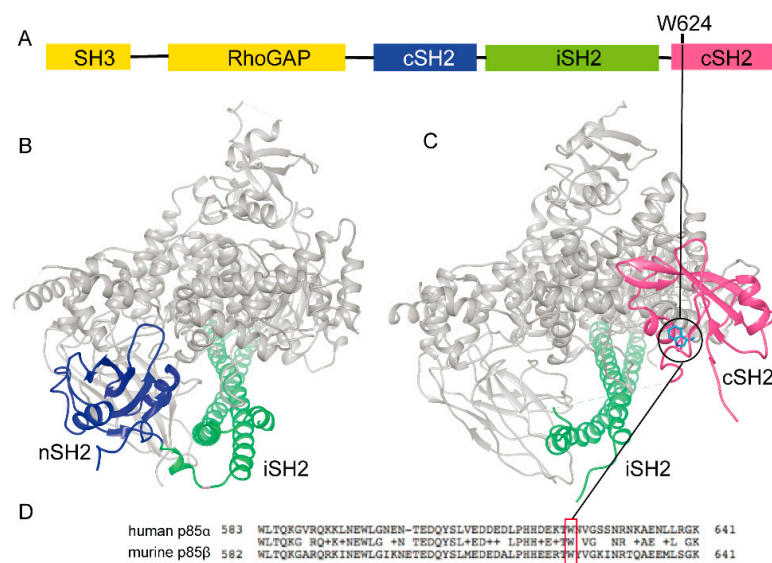


**Figure 4.** Crystal structures showing interaction of the p110 isoforms with the p85 isoforms in human and mouse PI3K. (A) Domain organization of p85 $\alpha$ . (B) Available crystal structure (PDB ID 4L1B) of human p110 $\alpha$  isoform with catalytic activity (grey) complexed with nSH2 (blue) and iSH2 (green) domains of human p85 $\alpha$ ; (C) available crystal structure (PDB ID 2Y3A) of mouse p110 $\beta$  in complex with iSH2 (green) and cSH2 (pink) domains of mouse p85 $\beta$ . (D) Alignment of the cSH2 domains of the human p85 $\alpha$  and mouse p85 $\beta$ ; homology is shown in the middle: W624 of the human p85 $\alpha$  protein is conserved and corresponds to the W616 of the mouse p85 $\beta$  protein (red box in D).

Regrettably, only the crystal structure of human p110 $\alpha$  in complex with nSH2 and iSH2 domains of p85 $\alpha$  is available (PDB ID 4L1B, Figure 4B). Hence, we explored the possible role of the amino-acid residue homologue to the W624 in mouse p85 being available in the crystal structure of mouse p110 $\beta$  isoform in complex with iSH2 and cSH2 domains of mouse p85 $\beta$  isoform (PDB ID 2Y3A, Figure 4C). Structure superimposition showed that mouse p85 $\beta$  shares common folds with the human p85 $\alpha$  counterpart. Sequence alignments demonstrated that human p85 $\alpha$  and mouse p85 $\beta$  display 73%

homology and 59% identity, whereas human p110 $\alpha$  and mouse p110 $\beta$  sequences have 57% homology and 40% identity. According to sequence alignment (Figure 4D), the W624 in the human p85 $\alpha$  corresponds to W616 in the mouse cSH2 domain of p85 $\beta$ . These data analyses showed that the W616 in the cSH2 domain of mouse p85 $\beta$  is not involved in the interaction between murine p85 $\beta$  and p110 $\beta$ . Thus, the structure-based prediction was inconclusive.

Thus, we carried out the functional assays (Figure 5) of the *PIK3R1*<sup>W624R</sup> in cells of the *PIK3R1*<sup>W624R</sup> carrying PDX line #475 ex vivo, by challenging the susceptibility to inhibitors of the PI3K/AKT/mTOR pathway that could be activated by suppression of the p85 $\alpha$  regulatory subunit and fruitfully targeted for therapy.

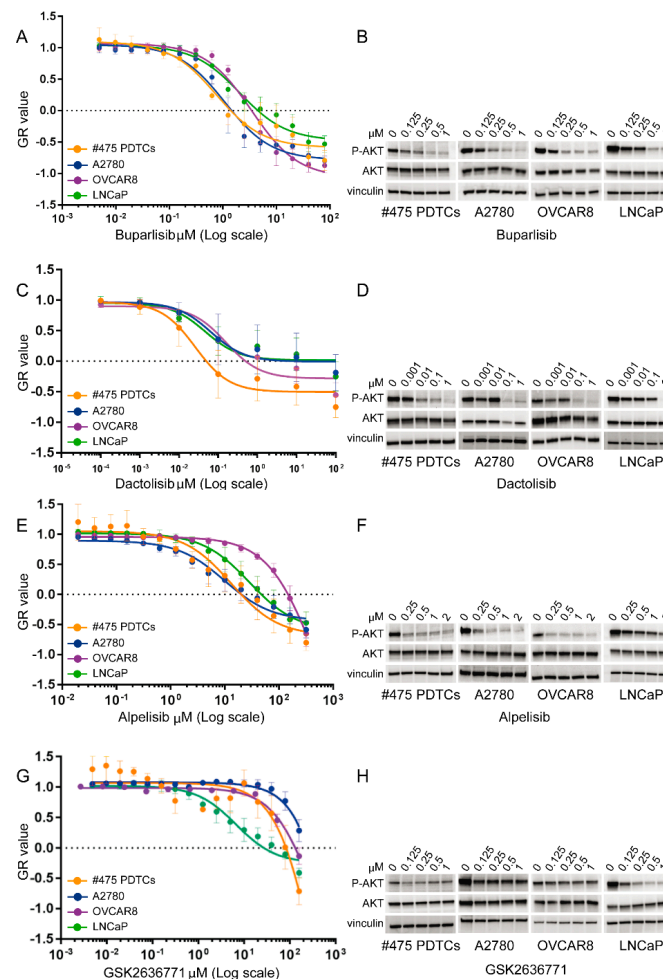


**Figure 5.** Response of *PIK3R1*<sup>W624R</sup> carrying PDTCs to inhibitors of the PI3K/AKT/mTOR pathway. In each experiment, control cell lines were assayed, too. (A,C,E,G): Dose-response curves in CellTiterGlo 72 h viability assays. Normalized growth rate (GR value) inhibition metrics of three replicate experiments is shown to take into account cell division rates. The sign of GR values relates directly to response phenotype: positive for partial growth inhibition, zero for complete cytostatic effect and negative for cytotoxicity. The x axis shows drug concentration on a log<sub>10</sub> (Log) scale. (B,D,F,H): Western blot analysis of the phosphorylation of the AKT signal transducer in response to drugs, as a proxy of PI3K activation status. (A) The *PIK3R1*<sup>W624R</sup> PDTCs showed susceptibility to the pan-class I PI3K inhibitor buparlisib (BKM120), comparable to that of the highly responsive A2780 cells; (C) the *PIK3R1*<sup>W624R</sup> PDTCs showed susceptibility to the dual PI3K/mTOR inhibitor dactolisib (BEZ235), comparable to that of the most sensitive (OVCAR-8) of the above cell lines; (E) the *PIK3R1*<sup>W624R</sup> PDTCs were also highly susceptible to the p110 $\alpha$  specific PI3K inhibitor alpelisib (BYL719) as well as the A2780 cells; and (G) resistant to the p110 $\beta$  specific inhibitor GSK2636771 to which the LNCaP cells are exquisitely susceptible.

To test cell susceptibility to drugs *ex vivo*, we propagated the PDX Derived Tumour Cells (PDTCs) depleted of mouse cells as short-term cultures. Viability assays were carried out by exposing PDTCs to inhibitors for 72 h. The susceptibility of *PIK3R1*<sup>W624R</sup> PDTCs was compared to that of the control cell lines (Figure 5) and to that of the PDTCs derived from the #2085 PDX line (Figure S3). The latter PDTCs were propagated from a bona fide HGS-EOC, carrying mutations of the *TP53* and *BRCA2* genes (Table S1), but not of genes involved in the PI3K/AKT/mTOR pathway. The following cell lines were assayed as controls, selected based on mutation spectrum (Cancer Cell Line Encyclopedia, <https://portals.broadinstitute.org/ccle>) and susceptibility or resistance to any given drug: A2780 ovarian carcinoma cells, carrying *PIK3CA* activating mutation and *PTEN* loss that make them highly sensitive to the pan-class I PI3K inhibitor buparlisib (BKM120), to the p110 $\alpha$  specific inhibitor alpelisib (BYL-719) and to the dual PI3K/mTOR inhibitor dactolisib (BEZ235); the OVCAR-8 ovarian carcinoma cells with wild-type *PIK3CA* and *TP53* gene mutation, but known to be susceptible to the dual PI3K/mTOR inhibitor dactolisib (BEZ235), as reported by the Genomic of Drug Sensitivity in Cancer Project (<https://www.cancerrxgene.org/>), and the *PTEN*-mutated LNCaP prostate carcinoma cells that are known to be exquisitely susceptible to the p110 $\beta$  specific inhibitor GSK2636771. To take into account cell division rates across the PDTCs and cell lines, growth rate inhibition metrics were used, i.e., GR-calculator [27].

The *PIK3R1*<sup>W624R</sup> #475 PDTCs but not the non-mutated #2085 PDTCs, were sensitive to the pan-class I PI3K inhibitor buparlisib (BKM120) as shown in Figure 5 and Figure S3, respectively. Figure 5 also shows the susceptibility of the *PIK3R1*<sup>W624R</sup> #475 PDTCs to the p110 $\alpha$  specific inhibitor alpelisib (BYL-719), compared to control cell lines. Similarly, these #475 PDTCs showed susceptibility to the dual PI3K and mTOR inhibitors dactolisib (BEZ235). Conversely, the p110 $\beta$  selective inhibitor GSK2636771 did not affect the *PIK3R1*<sup>W624R</sup> PDTCs. The susceptibility of *PIK3R1*<sup>W624R</sup> PDTCs to the four inhibitors was confirmed with a cytotoxicity assay (Figure S4). In line with the results of viability assays, buparlisib, dactolisib and alpelisib, but not GSK2636771, affected AKT phosphorylation (Figure 5), that is a proxy of PI3K activation status.

Moreover, *in vivo* buparlisib delayed the growth of the *PIK3R1*<sup>W624R</sup> PDXs (Figure 6A). As the total decrease of tumour volume could not allow proper estimation of possibly cytostatic agents, we demonstrated also the strong reduction of Ki67 positive, i.e., proliferating, cells in treated PDXs (Figure 7A,C). AKT phosphorylation was reduced in xenografts in line with growth delay by buparlisib treatment (Figure 6B). Accordingly, phosphorylation of the S6 protein, that is a proxy of the PI3K/AKT activation, was reduced (Figure 7B,D).

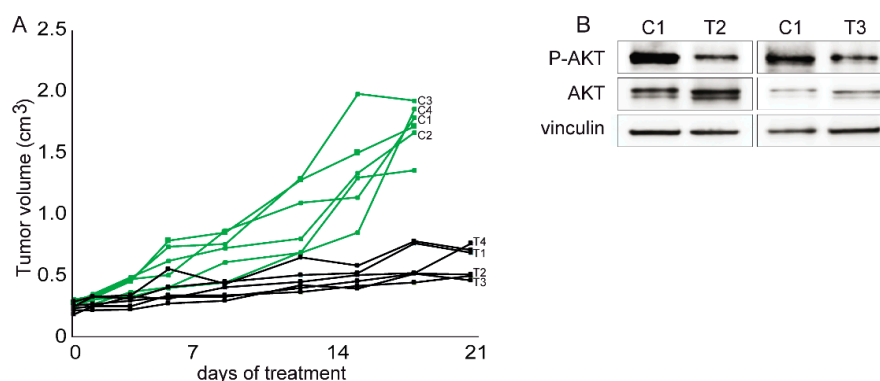


**Figure 6.** *In vivo* response of the *PIK3R1*<sup>W624R</sup> PDXs to buparlisib. Randomized mice were divided into two cohorts and treated with 20 mg/kg buparlisib, administered as described in the Methods section. (A) Growth curves of treated (black solid lines) and control (green solid lines) animals. (B) Western blot analysis of the phosphorylation of the AKT signal transducer in response to drugs, as a proxy of PI3K activation status in response to drugs, in the individual treated (T2 and T3) and control (C1) PDXs indicated in panel (A).

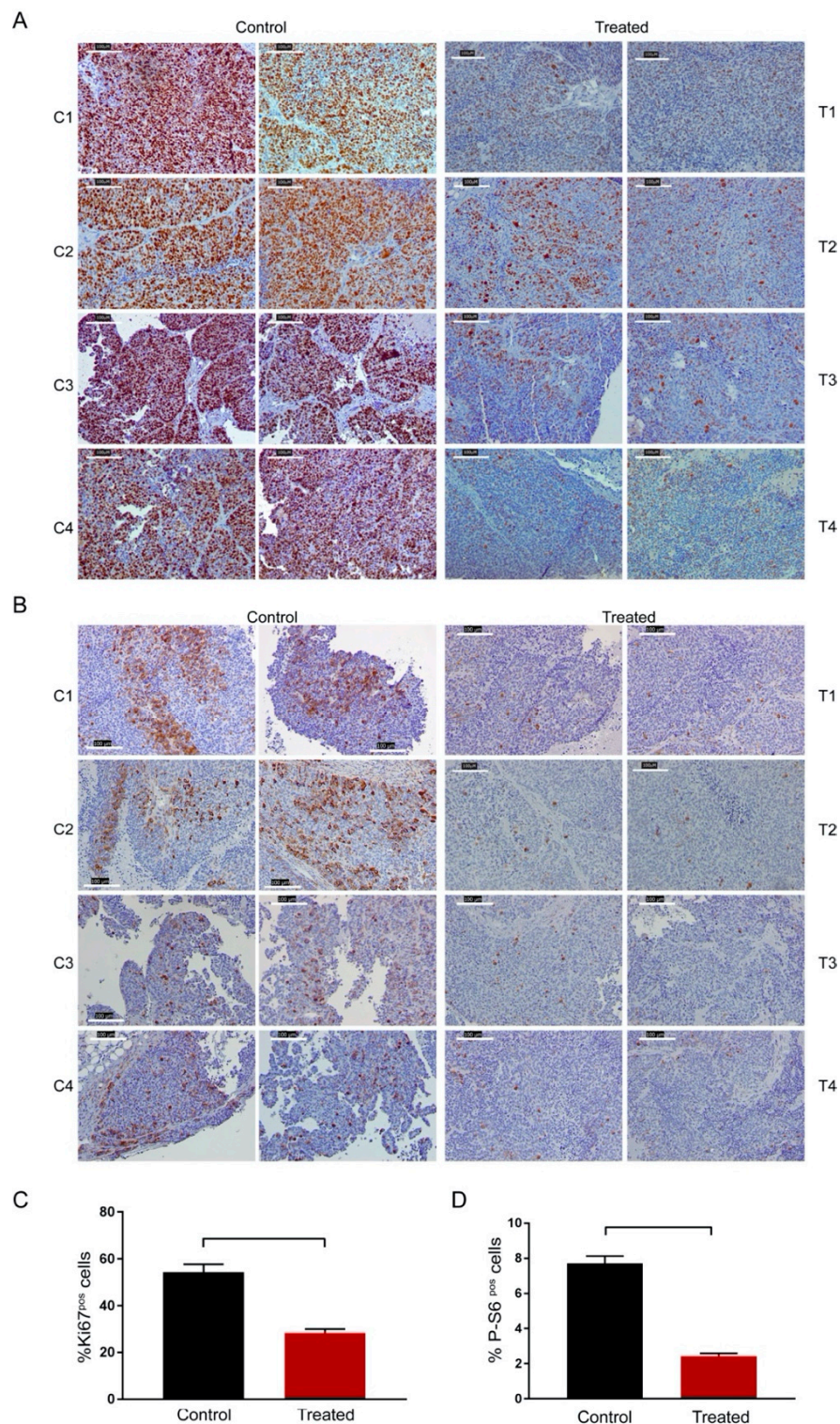


**Figure 7.** Immunohistochemical detection of proliferation index and decreased activation of PI3K in *PIK3R1*<sup>W624R</sup> PDXs, treated with buparlisib as shown in Figure 6. (A) Representative images of Ki67 positive cells detected in treated and control PDXs grown as shown in Figure 6 panel A; (B) representative images of P-S6 positive cells detected in treated and control PDXs grown as shown in Figure 6 panel A. (C) Quantification of Ki67 positive nuclei evaluated as a percentage of positive area versus total nuclei area. (D) Quantification of P-S6 positive cells evaluated as a percentage of positive area versus total area. The *p* value has been calculated using unpaired *t*-Student test.

#### 4. Discussion

We demonstrate here that a rare mutation in the *PIK3R1* tumour suppressor gene [29] is actionable in HGS-EOC using validated patient-derived models of the disease. *PIK3R1* is very frequently mutated in other cancer histotypes, with the notable exception of HGS-EOC [10], in particular in uterine carcinomas and carcinosarcomas, glioblastoma, breast and colorectal cancer. Most of the mutations reported so far are located in the iSH2 domain of the *PIK3R1* encoded p85 $\alpha$ , which is known to bind and regulate the p110 $\alpha$  subunit of PI3K [32]. The *PIK3R1*<sup>W624R</sup> mutation described here is located in the cSH2 domain of the p85 $\alpha$ . The same W624R amino acid change has been reported previously, but not characterized, in one colorectal cancer [34], while a W624C substitution has been reported in one non-small cell lung carcinoma (NSCLC) [35], and a nucleotide change in the same codon, leading to a non-sense mutation being found in one stomach cancer sample [36] and one endometrial carcinoma [37]. Other rare mutations in the cSH2 of the *PIK3R1* gene are reported in COSMIC (<https://cancer.sanger.ac.uk/cosmic>) and TumorPortal (<http://www.tumorportal.org>). The function of a number of these mutations has been studied in test tubes (see e.g., ref. [38]) or in functional assays in cell line models with totally different genetic backgrounds (see e.g., refs. [39,40]). As a result, the potential oncogenicity of only two mutations in the p85 $\alpha$  cSH2 domain has been proposed based on the promotion of survival and growth of Ba/F3, a murine interleukin-3 dependent pro-B cell line. On the other hand, in the cSH2 domain of the p85 $\alpha$ , several germline mutations are located, which in heterozygosity cause SHORT syndrome [41]. This syndrome is characterised by developmental defects and is historically defined by its acronym: Short stature (S), Hyperextensibility of joints and/or inguinal Hernia (H), Ocular depression (O), Rieger abnormality (R) and Teething delay (T). Molecular studies have shown that *PIK3R1* mutations associated with SHORT syndrome result in defects, and not in the activation of PI3K signalling [41,42].

Surprisingly, another mutation in the cSH2 domain (the R649W substitution) has been reported in both endometrial carcinoma and as a hotspot in four families affected by SHORT syndrome [42]. Therefore, although prediction algorithms allowed us to classify the W624R amino acid change in *PIK3R1* as possibly deleterious and damaging the protein product, it was difficult to predict its actual impact on ovarian cancer. As structure-based approaches are more specific than sequence-based approaches at predicting driver mutations [40], we endeavoured to model the association in p85 $\alpha$  between the W624R mutation and the p110 $\alpha$  subunit, but available crystal structures did not help in defining the impact of the *PIK3R1*<sup>W624R</sup> on human PI3K function. It has also been postulated that the role of the cSH2 domain of the human p85 $\alpha$  in oncogenesis relies on its interaction with and inhibition of the p110 $\beta$  isoform of the PI3K [43]. We disproved this hypothesis with functional assays *ex vivo* that showed directly the susceptibility *in vitro* of *PIK3R1*<sup>W624R</sup> PTDCs to the p110 $\alpha$  specific inhibitor alpelisib but not to the p110 $\beta$  specific inhibitor. Susceptibility to pathway inhibition was confirmed by treating PDTCs with a dual PI3K/mTOR inhibitor and with the pan class I PI3K inhibitor buparlisib, which also inhibited the growth of PDXs *in vivo*. These data confirmed the requirement of proper functional assays for evaluating the driving oncogenic effect of any given mutation.

Other observations suggest that the impact of any mutation as well as its actionability could be better studied in patient-derived models and in the actual tissue affected. Nowadays, the traditional system of anatomic cancer classification has been overcome by a classification system based on molecular alterations shared by tumours across diverse tissue types. This concept has led to the development of so-called basket or umbrella trials. However, exceptions that challenge this concept have also become apparent from such notable examples as the unpredictable clinical responses to a potent BRAF inhibitor across diverse malignancies, all expressing the same BRAF mutation [44].

Altogether, the data show that, to assess the function of mutant alleles, assays in patient-derived models of the relevant cancer, such as PDXs and short-term PDTCs, are extremely important. Long-term cultures of patients' samples [45] are useful for drug screening. Short-term monolayer cultures [46] and organoids [47] derived from patients' biopsies have been shown as a valuable model for rapid drug testing and thus for co-clinical trials, but their application may be limited by the modest take and

throughput, respectively. Thus, all the patient-derived experimental models should be considered complementary and not alternative, as every model system is imperfect and suitable in its own way.

The validation of *PIK3R1*<sup>W624R</sup> as a biomarker of response to PI3K/AKT/mTOR pathway inhibitors exceeds the aim of this work. The PI3K-AKT-mTOR signalling pathway is one of the most frequently dysregulated ones in human cancers. More than 40 inhibitors of this pathway have reached various stages of clinical development, but only a few have been approved by FDA and EMA [48]. In clinical studies, inhibitors of the pathway have shown limited efficacy and/or manageability [20]. P110 isoform-specific inhibitors appear more promising in trials [49–51]. In ovarian cancer, gene abnormalities other than homologous recombination defects are even more difficult to pair with an approved or investigational drug [52].

## 5. Conclusions

In the ovarian cancer field, suitable preclinical models such as PDXs are still invaluable for population-based studies, as they might better mimic the inter-tumour heterogeneity that is seen in patients and might be predictive of the clinical efficacy of targeted drugs. This model allowed us to identify a rare mutation in the *PIK3R1* gene in a domain that was not expected to be involved in oncogenesis, and showing that this mutation makes ovarian cancer cells responsive to inhibitors of the PI3K/AKT/mTOR pathway.

**Supplementary Materials:** The following are available online at <http://www.mdpi.com/2073-4409/9/2/442/s1>, Supplementary Methods Part 1: additional methodological details of animal experimentation, Supplementary Methods Part 2: completed ARRIVE checklist, Figure S1: Pipeline of WES and SNP data analyses, Figure S2: Expression of P-S6 as proxy of PI3K activation in PDX lines, Figure S3: Comparison between the response of the *PIK3R1*<sup>W624R</sup> carrying PDXs and non-mutated PDXs to the pan-class I PI3K inhibitor buparlisib, Figure S4 Cytostatic/cytotoxic effects of PI3K pathway inhibitors on *PIK3R1*<sup>W624R</sup> carrying PDXs and control cell lines evaluated using crystal violet staining, Table S1: List and molecular characterization of 43 PDX lines propagated from EOC samples, Table S2: Clinical information of the patients who donated the 12 samples of HGS-EOC that were studied in-depth with WES and SNP arrays, Table S3: CNAs detected in cancer genes in the 12 PDX lines studied in depth compared to CNAs reported in TCGA analysis of HGS-EOC (A) comparison between CNAs found in the PDX lines and CNAs reported in TCGA for HGS-EOC (B) CNAs of the genes found amplified in more than 10% of the HGS-EOCs reported in TCGA, detected in the 12 PDX lines, Table S4: Single Nucleotide Variants (SNV) in cancer genes found in PDX lines derived from naïve HGS-EOC comprising those classified as SNPs, Table S5: Primers and conditions used for pyrosequencing samples of human source tumours of PDXs with *PIK3R1*<sup>W624R</sup> mutation.

**Author Contributions:** Conceptualization, M.F.D.R. and M.O.; Data curation, G.M., E.G., R.A.C., G.V. and M.O.; Formal analysis, J.E., R.A.C., G.V. and M.O.; Funding acquisition, R.A.C., J.D.B. and M.F.D.R.; Investigation, C.D., J.E., M.A., S.C., S.P., M.R., E.M., G.D.N., E.B., T.V., D.H., M.J.-L., A.L.P. and M.O.; Methodology, C.D., J.E., M.A., G.D.N., E.B., T.V. and M.O.; Resources, F.B., D.K., R.P., M.V. and G.V.; Software, R.A.C.; Supervision, G.V. and M.F.D.R.; Visualization, C.D., J.E., M.F.D.R. and M.O.; Writing—original draft, G.V., M.F.D.R. and M.O.; Writing—review and editing, J.D.B., M.F.D.R. and M.O. All authors have read and agreed to the published version of the manuscript.

**Funding:** This work has been supported by the Italian Ministry of Health, Ricerca Corrente 2018, by the Italian Association for Cancer Research (AIRC) IG grant 2015 number 17473 and FPRC 5xmille Ministero della Salute 2015 (Strategy Project) to M.F.D. and by the EPIGEN FLAG PROJECT to R.A.C., J.D.B. acknowledges funding and support from Cancer Research UK (grant number A15601), the University of Cambridge, National Institute for Health Research Cambridge Biomedical Research Centre and Hutchison Whampoa Limited. The funders had no role in study design, data collection and analysis, decision to publish or preparation of the manuscript.

**Acknowledgments:** We thank the Pathology Department of the Candiolo Cancer Institute and the Biorepository and Histopathology Core Facilities of the Cancer Research UK Cambridge Institute for technical support. E.B. is the recipient of a PhD fellowship under the funding of “Dipartimenti di Eccellenza 2018-2022” (Project no. D15D18000410001) of the Department of Medical Sciences of the University of Turin.

**Conflicts of Interest:** The authors declare no competing interests.

## References

1. Kurman, R.J.; Shih, I.-M. Molecular pathogenesis and extraovarian origin of epithelial ovarian cancer—Shifting the paradigm. *Hum. Pathol.* **2011**, *42*, 918–931. [[CrossRef](#)] [[PubMed](#)]
2. Bowtell, D.D.; Böhm, S.; Ahmed, A.A.; Aspuria, P.-J.; Bast, R.C.; Beral, V.; Berek, J.S.; Birrer, M.J.; Blagden, S.; Bookman, M.A.; et al. Rethinking ovarian cancer II: Reducing mortality from high-grade serous ovarian cancer. *Nat. Rev. Cancer* **2015**, *15*, 668–679. [[CrossRef](#)] [[PubMed](#)]
3. Jayson, G.C.; Kohn, E.C.; Kitchener, H.C.; Ledermann, J.A. Ovarian cancer. *Lancet* **2014**, *384*, 1376–1388. [[CrossRef](#)]
4. Pujade-Lauraine, E.; Ledermann, J.A.; Selle, F.; Gebiski, V.; Penson, R.T.; Oza, A.M.; Korach, J.; Huzarski, T.; Poveda, A.; Pignata, S.; et al. Olaparib tablets as maintenance therapy in patients with platinum-sensitive, relapsed ovarian cancer and a BRCA1/2 mutation (SOLO2/ENGOT-Ov21): A double-blind, randomised, placebo-controlled, phase 3 trial. *Lancet Oncol.* **2017**, *18*, 1274–1284. [[CrossRef](#)]
5. Moore, K.; Colombo, N.; Scambia, G.; Kim, B.-G.; Oaknin, A.; Friedlander, M.; Lisysanskaya, A.; Floquet, A.; Leary, A.; Sonke, G.S.; et al. Maintenance Olaparib in Patients with Newly Diagnosed Advanced Ovarian Cancer. *New Engl. J. Med.* **2018**, *379*, 2495–2505. [[CrossRef](#)] [[PubMed](#)]
6. Hyman, D.M.; Taylor, B.S.; Baselga, J. Implementing Genome-Driven Oncology. *Cell* **2017**, *168*, 584–599. [[CrossRef](#)]
7. Patch, A.M.; Christie, E.L.; Etemadmoghadam, D.; Garsed, D.W.; George, J.; Fereday, S.; Nones, K.; Cowin, P.; Alsop, K.; Bailey, P.J.; et al. Whole-genome characterization of chemoresistant ovarian cancer. *Nature* **2015**, *521*, 489–494. [[CrossRef](#)]
8. The Cancer Genome Atlas Research Network. Integrated genomic analyses of ovarian carcinoma. *Nature* **2011**, *474*, 609–615. [[CrossRef](#)]
9. Garraway, L.A.; Lander, E.S. Lessons from the Cancer Genome. *Cell* **2013**, *153*, 17–37. [[CrossRef](#)]
10. Chang, M.T.; Bhattarai, T.S.; Schram, A.M.; Bielski, C.M.; Donoghue, M.T.; Jonsson, P.; Chakravarty, D.; Phillips, S.; Kandoth, C.; Penson, A.; et al. Accelerating Discovery of Functional Mutant Alleles in Cancer. *Cancer Discov.* **2018**, *8*, 174–183. [[CrossRef](#)]
11. Erriquez, J.; Olivero, M.; Mittica, G.; Scalzo, M.S.; Vaira, M.; De Simone, M.; Ponzzone, R.; Katsaros, D.; Aglietta, M.; Calogero, R.; et al. Xenopatient show the need for precision medicine approach to chemotherapy in ovarian cancer. *Oncotarget* **2016**, *7*, 26181–26191. [[CrossRef](#)] [[PubMed](#)]
12. Dobbin, Z.C.; Katre, A.A.; Steg, A.D.; Erickson, B.K.; Shah, M.M.; Alvarez, R.D.; Conner, M.G.; Schneider, D.; Chen, N.; Landen, C.N. Using heterogeneity of the patient-derived xenograft model to identify the chemoresistant population in ovarian cancer. *Oncotarget* **2014**, *5*, 8750–8764. [[CrossRef](#)] [[PubMed](#)]
13. Weroha, S.J.; Becker, M.A.; Enderica-Gonzalez, S.; Harrington, S.C.; Oberg, A.L.; Maurer, M.J.; Perkins, S.E.; Al Hilli, M.; Butler, K.A.; McKinstry, S.; et al. Tumorgrafts as in vivo surrogates for women with ovarian cancer. *Clin. Cancer Res.* **2014**, *20*, 1288–1297. [[CrossRef](#)] [[PubMed](#)]
14. Topp, M.D.; Hartley, L.; Cook, M.; Heong, V.; Boehm, E.; McShane, L.; Pyman, J.; McNally, O.; Ananda, S.; Harrell, M.; et al. Molecular correlates of platinum response in human high-grade serous ovarian cancer patient-derived xenografts. *Mol. Oncol.* **2014**, *8*, 656–668. [[CrossRef](#)] [[PubMed](#)]
15. Liu, J.F.; Palakurthi, S.; Zeng, Q.; Zhou, S.; Ivanova, E.; Huang, W.; Zervantonakis, I.K.; Selfors, L.M.; Shen, Y.; Pritchard, C.C.; et al. Establishment of Patient-Derived Tumor Xenograft Models of Epithelial Ovarian Cancer for Preclinical Evaluation of Novel Therapeutics. *Clin. Cancer Res.* **2017**, *23*, 1263–1273. [[CrossRef](#)] [[PubMed](#)]
16. Cybulska, P.; Stewart, J.M.; Sayad, A.; Virtanen, C.; Shaw, P.A.; Clarke, B.; Stickle, N.; Bernardini, M.Q.; Neel, B.G. A Genomically Characterized Collection of High-Grade Serous Ovarian Cancer Xenografts for Preclinical Testing. *Am. J. Pathol.* **2018**, *188*, 1120–1131. [[CrossRef](#)]
17. Ricci, F.; Bizzaro, F.; Cesca, M.; Guffanti, F.; Ganzinelli, M.; Decio, A.; Ghilardi, C.; Perego, P.; Fruscio, R.; Buda, A.; et al. Patient-Derived Ovarian Tumor Xenografts Recapitulate Human Clinicopathology and Genetic Alterations. *Cancer Res.* **2014**, *74*, 6980–6990. [[CrossRef](#)]
18. Colombo, P.-E.; Du Manoir, S.; Orsetti, B.; Bras-Gonçalves, R.; Lambros, M.B.; Mackay, A.; Nguyen, T.-T.; Boissière, F.; Pourquier, D.; Bibeau, F.; et al. Ovarian carcinoma patient derived xenografts reproduce their tumor of origin and preserve an oligoclonal structure. *Oncotarget* **2015**, *6*, 28327–28340. [[CrossRef](#)]

19. Sartore-Bianchi, A.; Trusolino, L.; Martino, C.; Bencardino, K.; Lonardi, S.; Bergamo, F.; Zagonel, V.; Leone, F.; Depetris, I.; Martinelli, E.; et al. Dual-targeted therapy with trastuzumab and lapatinib in treatment-refractory, KRAS codon 12/13 wild-type, HER2-positive metastatic colorectal cancer (HERACLES), a proof-of-concept, multicentre, open-label, phase 2 trial. *Lancet Oncol.* **2016**, *17*, 738–746. [[CrossRef](#)]
20. Janku, F.; Yap, T.A.; Meric-Bernstam, F. Targeting the PI3K pathway in cancer: Are we making headway? *Nat. Rev. Clin. Oncol.* **2018**, *15*, 273–291. [[CrossRef](#)]
21. Ben-David, U.; Ha, G.; Tseng, Y.-Y.; Greenwald, N.F.; Oh, C.; Shih, J.; McFarland, J.M.; Wong, B.; Boehm, J.S.; Beroukhi, R.; et al. Patient-derived xenografts undergo mouse-specific tumor evolution. *Nat. Genet.* **2017**, *49*, 1567–1575. [[CrossRef](#)] [[PubMed](#)]
22. Meehan, T.F.; Conte, N.; Goldstein, T.C.; Inghirami, G.; Murakami, M.A.; Brabetz, S.; Gu, Z.; Wiser, J.A.; Dunn, P.; Begley, D.A.; et al. PDX-MI: Minimal Information for Patient-Derived Tumor Xenograft Models. *Cancer Res.* **2017**, *77*, e62–e66. [[CrossRef](#)] [[PubMed](#)]
23. Baralis, E.; Bertotti, A.; Fiori, A.; Grand, A. LAS: A Software Platform to Support Oncological Data Management. *J. Med. Syst.* **2012**, *36*, 81–90. [[CrossRef](#)] [[PubMed](#)]
24. Krepler, C.; Xiao, M.; Sproesser, K.; Brafford, P.A.; Shannan, B.; Beqiri, M.; Liu, Q.; Xu, W.; Garman, B.; Nathanson, K.L.; et al. Personalized Preclinical Trials in BRAF Inhibitor-Resistant Patient-Derived Xenograft Models Identify Second-Line Combination Therapies. *Clin. Cancer Res.* **2016**, *22*, 1592–1602. [[CrossRef](#)]
25. Sapino, A.; Marchiò, C.; Senetta, R.; Castellano, I.; Macrì, L.; Cassoni, P.; Ghisolfi, G.; Cerrato, M.; D'Ambrosio, E.; Bussolati, G. Routine assessment of prognostic factors in breast cancer using a multicore tissue microarray procedure. *Virchows Arch.* **2006**, *449*, 288–296. [[CrossRef](#)]
26. Butler, K.A.; Hou, X.; Becker, M.A.; Zanfagnin, V.; Enderica-Gonzalez, S.; Visscher, D.; Kalli, K.R.; Tienchaianada, P.; Haluska, P.; Weroha, S.J. Prevention of Human Lymphoproliferative Tumor Formation in Ovarian Cancer Patient-Derived Xenografts. *Neoplasia* **2017**, *19*, 628–636. [[CrossRef](#)]
27. Hafner, M.; Niepel, M.; Chung, M.; Sorger, P.K. Growth rate inhibition metrics correct for confounders in measuring sensitivity to cancer drugs. *Nat. Methods* **2016**, *13*, 521–527. [[CrossRef](#)]
28. Forbes, S.A.; Bindal, N.; Bamford, S.; Cole, C.; Kok, C.Y.; Beare, D.; Jia, M.; Shepherd, R.; Leung, K.; Menzies, A.; et al. COSMIC, mining complete cancer genomes in the Catalogue of Somatic Mutations in Cancer. *Nucleic Acids Res.* **2011**, *39*, D945–D950. [[CrossRef](#)]
29. Berger, A.C.; Korkut, A.; Kanchi, R.S.; Hegde, A.M.; Lenoir, W.; Liu, W.; Liu, Y.; Fan, H.; Shen, H.; Ravikumar, V.; et al. A Comprehensive Pan-Cancer Molecular Study of Gynecologic and Breast Cancers. *Cancer Cell* **2018**, *33*, 690–705. [[CrossRef](#)]
30. Hassan, M.S.; Shaalan, A.A.; Dessouky, M.I.; Abdelnaiem, A.E.; ElHefnawi, M. Evaluation of computational techniques for predicting non-synonymous single nucleotide variants pathogenicity. *Genomics* **2018**, *111*, 869–882. [[CrossRef](#)]
31. Wagner, A.H.; Coffman, A.C.; Ainscough, B.J.; Spies, N.C.; Skidmore, Z.L.; Campbell, K.M.; Krysiak, K.; Pan, D.; McMichael, J.F.; Eldred, J.M.; et al. DGIdb 2.0, mining clinically relevant drug-gene interactions. *Nucleic Acids Res.* **2016**, *44*, D1036–D1044. [[CrossRef](#)] [[PubMed](#)]
32. Cheung, L.W.; Mills, G.B. Targeting therapeutic liabilities engendered by PIK3R1 mutations for cancer treatment. *Pharmacogenomics* **2016**, *17*, 297–307. [[CrossRef](#)] [[PubMed](#)]
33. McPherson, A.; Roth, A.; Laks, E.; Masud, T.; Bashashati, A.; Zhang, A.W.; Ha, G.; Biele, J.; Yap, D.; Wan, A.; et al. Divergent modes of clonal spread and intraperitoneal mixing in high-grade serous ovarian cancer. *Nat. Genet.* **2016**, *48*, 758–767. [[CrossRef](#)] [[PubMed](#)]
34. Giannakis, M.; Mu, X.J.; Shukla, S.A.; Qian, Z.R.; Cohen, O.; Nishihara, R.; Bahl, S.; Cao, Y.; Amin-Mansour, A.; Yamauchi, M.; et al. Genomic Correlates of Immune-Cell Infiltrates in Colorectal Carcinoma. *Cell Rep.* **2016**, *15*, 857–865. [[CrossRef](#)]
35. Campbell, J.D.; Alexandrov, A.; Kim, J.; Wala, J.; Berger, A.H.; Peadarallu, C.S.; Shukla, S.A.; Guo, G.; Brooks, A.N.; Murray, B.A.; et al. Distinct patterns of somatic genome alterations in lung adenocarcinomas and squamous cell carcinomas. *Nat. Genet.* **2016**, *48*, 607–616. [[CrossRef](#)]
36. Wang, K.; Yuen, S.T.; Xu, J.; Lee, S.P.; Yan, H.H.N.; Shi, S.T.; Siu, H.C.; Deng, S.; Chu, K.M.; Law, S.; et al. Whole-genome sequencing and comprehensive molecular profiling identify new driver mutations in gastric cancer. *Nat. Genet.* **2014**, *46*, 573–582. [[CrossRef](#)]



37. Soumerai, T.E.; Donoghue, M.T.; Bandlamudi, C.; Srinivasan, P.; Chang, M.T.; Zamarin, D.; Cadoo, K.A.; Grisham, R.N.; O’Cearbhaill, R.E.; Tew, W.P.; et al. Clinical Utility of Prospective Molecular Characterization in Advanced Endometrial Cancer. *Clin. Cancer Res.* **2018**, *24*, 5939–5947. [[CrossRef](#)]
38. Jaiswal, B.S.; Janakiraman, V.; Kljavin, N.M.; Chaudhuri, S.; Stern, H.M.; Wang, W.; Kan, Z.; Dbouk, H.A.; Peters, B.A.; Waring, P.; et al. Somatic mutations in p85alpha promote tumorigenesis through class IA PI3K activation. *Cancer Cell* **2009**, *16*, 463–474. [[CrossRef](#)]
39. Ng, P.K.S.; Li, J.; Jeong, K.J.; Shao, S.; Chen, H.; Tsang, Y.H.; Sengupta, S.; Wang, Z.; Bhavana, V.H.; Tran, R.; et al. Systematic Functional Annotation of Somatic Mutations in Cancer. *Cancer Cell* **2018**, *33*, 450–462. [[CrossRef](#)]
40. Bailey, M.H.; Tokheim, C.; Porta-Pardo, E.; Sengupta, S.; Bertrand, D.; Weerasinghe, A.; Colaprico, A.; Wendl, M.C.; Kim, J.; Reardon, B.; et al. Comprehensive Characterization of Cancer Driver Genes and Mutations. *Cell* **2018**, *173*, 371–385. [[CrossRef](#)]
41. Avila, M.; Dymont, D.A.; Sagen, J.V.; St-Onge, J.; Moog, U.; Chung, B.H.; Mo, S.; Mansour, S.; Albanese, A.; Garcia, S.; et al. Clinical reappraisal of SHORT syndrome with PIK3R1 mutations, toward recommendation for molecular testing and management. *Clin. Genet.* **2016**, *89*, 501–506. [[CrossRef](#)] [[PubMed](#)]
42. Thauvin-Robinet, C.; Auclair, M.; Duplomb, L.; Caron-Debarle, M.; Avila, M.; St-Onge, J.; Le Merrer, M.; Le Luyer, B.; Héron, D.; Mathieu-Dramard, M.; et al. PIK3R1 Mutations Cause Syndromic Insulin Resistance with Lipoatrophy. *Am. J. Hum. Genet.* **2013**, *93*, 141–149. [[CrossRef](#)] [[PubMed](#)]
43. Zhang, X.; Vadas, O.; Perisic, O.; Anderson, K.E.; Clark, J.; Hawkins, P.T.; Stephens, L.R.; Williams, R.L. Structure of Lipid Kinase p110β/p85β Elucidates an Unusual SH2-Domain-Mediated Inhibitory Mechanism. *Mol. Cell* **2011**, *41*, 567–578. [[CrossRef](#)] [[PubMed](#)]
44. Hyman, D.M.; Puzanov, I.; Subbiah, V.; Faris, J.E.; Chau, I.; Blay, J.-Y.; Wolf, J.; Raje, N.S.; Diamond, E.L.; Hollebecque, A.; et al. Vemurafenib in Multiple Nonmelanoma Cancers with BRAF V600 Mutations. *New Engl. J. Med.* **2015**, *373*, 726–736. [[CrossRef](#)] [[PubMed](#)]
45. Crystal, A.S.; Shaw, A.T.; Sequist, L.V.; Friboulet, L.; Niederst, M.J.; Lockerman, E.L.; Frias, R.L.; Gainor, J.F.; Amzallag, A.; Greninger, P.; et al. Patient-derived models of acquired resistance can identify effective drug combinations for cancer. *Science* **2014**, *346*, 1480–1486. [[CrossRef](#)] [[PubMed](#)]
46. Kodack, D.P.; Farago, A.F.; Dastur, A.; Held, M.A.; Dardaei, L.; Friboulet, L.; Von Flotow, F.; Damon, L.J.; Lee, D.; Parks, M.; et al. Primary Patient-Derived Cancer Cells and Their Potential for Personalized Cancer Patient Care. *Cell Rep.* **2017**, *21*, 3298–3309. [[CrossRef](#)]
47. Hill, S.J.; Decker, B.; Roberts, E.A.; Horowitz, N.S.; Muto, M.G.; Worley, M.J.; Feltmate, C.M.; Nucci, M.R.; Swisher, E.M.; Nguyen, H.; et al. Prediction of DNA Repair Inhibitor Response in Short-Term Patient-Derived Ovarian Cancer Organoids. *Cancer Discov.* **2018**, *8*, 1404–1421. [[CrossRef](#)]
48. Hanker, A.B.; Kaklamani, V.; Arteaga, C.L. Challenges for the Clinical Development of PI3K Inhibitors: Strategies to Improve Their Impact in Solid Tumors. *Cancer Discov.* **2019**, *9*, 482–491. [[CrossRef](#)]
49. André, F.; Ciruelos, E.; Rubovszky, G.; Campone, M.; Loibl, S.; Rugo, H.S.; Iwata, H.; Conte, P.; Mayer, I.A.; Kaufman, B.; et al. Alpelisib for PIK3CA-Mutated, Hormone Receptor-Positive Advanced Breast Cancer. *New Engl. J. Med.* **2019**, *380*, 1929–1940. [[CrossRef](#)]
50. Juric, D.; Rodon, J.; Tabernero, J.; Janku, F.; Burris, H.A.; Schellens, J.H.; Middleton, M.R.; Berlin, J.; Schuler, M.; Gil-Martin, M.; et al. Phosphatidylinositol 3-Kinase α-Selective Inhibition With Alpelisib (BYL719) in PIK3CA-Altered Solid Tumors: Results From the First-in-Human Study. *J. Clin. Oncol.* **2018**, *36*, 1291–1299. [[CrossRef](#)]
51. Mateo, J.; Ganji, G.; Lemech, C.; Burris, H.A.; Han, S.-W.; Swales, K.; Decordova, S.; Deyoung, M.P.; Smith, D.A.; Kalyana-Sundaram, S.; et al. A First-Time-in-Human Study of GSK2636771, a Phosphoinositide 3 Kinase Beta-Selective Inhibitor, in Patients with Advanced Solid Tumors. *Clin. Cancer Res.* **2017**, *23*, 5981–5992. [[CrossRef](#)] [[PubMed](#)]
52. Barroilhet, L.; Matulonis, U. The NCI-MATCH trial and precision medicine in gynecologic cancers. *Gynecol. Oncol.* **2018**, *148*, 585–590. [[CrossRef](#)] [[PubMed](#)]

